respectively, of added complex, is linear, the intercept ($k_{cat_{max}} = k_{cat'} + k_{cat}$) being 3.0×10^{-2} s^{-1} and slope ($-k_{M_{TOT}} = -(k_{M'} + k_M)$) being 1.0×10^{-3} M, consistent with the process in Scheme II. Such plots from use of only the basic form of the complex (i.e., [**8**]) are decidely nonlinear and indicate that it alone is not responsible for *p*NPP binding and hydrolysis.

Conclusion

Although one can never be certain that conclusions drawn from model studies can be extrapolated to the enzymic systems, we believe this tris(imidazolyl)phosphine oxide provides several important small-molecule precedents for observations made with carbonic anhydrase.

(1) Ligand **2b**, when bound to equimolar Zn(II) or Co(II), promotes the dissociation of a metal-bound H_2O having pK_as of ~6 and 7.8, respectively. Spectrophotometric evidence for the Co(II) complex indicates that titration of the Co–OH_2 reduces the coordination around the metal from 6 to 5 or 4 as evidenced by the characteristic absorption spectrum of the basic form of the complex.

(2) Monovalent anions such as halides, NO_3^-, and CH_3COO^- interact with the Co(II) complex to produce unique 4- (5-) coordinate complexes, similar to the situation in Co(II)CA. ClO_4^- appears not to be able to associate strongly enough to the complex to produce a characteristic species.

(3) As a function of pH, the absorption spectra of the Co(II)·**2b** complexes in the presence of various anions invariably change at high pH to that of the basic form of the complex. One observes that the spectrophotometric pK_a of the Co(II) complex is shifted to higher values in the presence of anions. The observation clearly stems from a mass action effect whereby the anion is displaced from the metal by increasing concentrations of OH^-. Certain anions such as picolinate associate with the complex so strongly that very high [OH^-] is required to displace them. These observations based on the model system explain in a straightforward way the analogous situation in Co(II)CA; the inhibition of catalysis by the enzyme by monovalent anions may be likewise explained.

(4) Zn(II)·**2b** will catalyze the interconversion of CO_2 and HCO_3^-, although very inefficiently. It is clear that the simple expectation that catalysts employing low M^{2+} coordination numbers and a metal-bound hydroxide alone are sufficient to lead to enormous rate accelerations for this process is an oversimplified one. Since our previous catalyst, [tris[4,5-diisopropyl-2-imidazolyl]phosphine]zinc(2+) was more active for this process than Zn(II)·**2b** and considerably more strained, it may be that severe distortion in the complex is required for optimal rates. Of course one cannot overlook the possibility that the enzyme provides a requisite H-bonding network that cannot be duplicated in these models.

(5) **2b**·Co(II) will catalyze the hydrolysis of *p*-nitrophenyl picolinate. Nonlinearity of plots of k_{obsd} vs. [**2b**·Co(II)] in either its total or basic form indicates preequilibrium binding of complex and pNPP.

Acknowledgment. We gratefully acknowledge the financial assistance of the National Science and Engineering Research Council of Canada, The University of Alberta, and the donors of the Petroleum Research Fund, administered by the American Chemical Society, for partial support of the latter stages of this research. Helpful discussions with Professors H. B. Dunford and W. Bridger (Department of Biochemistry, University of Alberta) are also gratefully acknowledged, as are the comments of the referees.

Registry No. **2b**, 81293-76-7; **3**, 81277-92-1; **5**, 74104-89-5; Co, 7440-48-4; Zn, 7440-66-6; 2,4,5-trimethylimidazole, 822-90-2.

Electron Delocalization in Mixed-Valence Molybdenum Polyanions

C. Sanchez,[1a] J. Livage,[1a] J. P. Launay,*[1b] M. Fournier,[1b] and Y. Jeannin[1b]

Contribution from Laboratoire de Spectrochime du Solide and Laboratoire de Chimie des Mêtaux de Transition, Universitê Pierre et Marie Curie, 75230 Paris Cedex 05, France.
Received June 3, 1981

Abstract: Electron transfer in mixed-valence molybdenum polyanions has been studied by ESR and optical spectroscopy. Two series of compounds belonging to the Lindqvist (Mo_6O_{19}) and the Keggin ($XMo_{12}O_{40}$) structural types have been considered. The degree of valence trapping and ground-state delocalization have been measured by ESR at very low temperature (4 K). Optical activation energies have been deduced from the position of intervalence transfer absorption bands. Thermal activation energies have been measured from a detailed analysis of the ESR line width and line shape within the 4–200-K temperature range. Values of the transfer integral *J* between adjacent molybdenum sites have been estimated from a comparison between optical and thermal activation energies. Experiments show that all of the studied polyanions belong to class II of mixed-valence compounds. Thermally activated electron hopping appears to be much easier in the Keggin structure than in the Lindqvist structure.

A number of hetero- and isopolyanions of molybdenum are reducible to a series of mixed-valence compounds commonly named "heteropoly blues" containing Mo^{VI} and Mo^{V}. These species exhibit intense intervalence transfer bands and occasionally ESR signals that have been interpreted by assuming electron trapping at low temperature.[1c,2] This description of the electronic structure corresponds to class II systems in Robin and Day's classification[3] of mixed-valence compounds. For such systems, two closely related electron transfer processes can occur: (i) a thermal electron transfer, analogous to the so-called "hopping" process in solids, and (ii) an optical electron transfer. If the electronic interaction between metal centers is vanishing, it has been shown by Hush[4] that the thermal activation energy (E_{th}) should be one-fourth of the optical energy (E_{op}). For nonzero

(1) (a) Laboratoire de Spectrochimie du Solide. (b) Laboratoire de Chimie des Mêtaux de Transition. (c) Prados, R. A.; Meiklejohn, P. T.; Pope, M. T. *J. Am. Chem. Soc.* **1974**, *96*, 1261.
(2) Prados, R. A.; Pope, M. T. *Inorg. Chem.* **1976**, *15*, 2547.
(3) Robin, M. B.; Day, P. *Adv. Inorg. Chem. Radiochem.* **1967**, *10*, 248.
(4) Hush, N. S. *Prog. Inorg. Chem.* **1967**, *8*, 391.

0002-7863/82/1504-3194$01.25/0

electronic interaction, the thermal activation energy is expected to be lower than this limit as shown by[5]

$$E_{th} = {}^1/_4E_{op} - J + (J^2/E_{op}) \quad (1)$$

where J is the electron transfer integral.

Several studies have already dealt with the ESR of Mo^V-containing polyanions.[1c,2,6-14] However, it is only recently that the hyperfine structure due to the coupling with ^{95}Mo and ^{97}Mo (both $I = {}^5/_2$) has been observed and correctly interpreted. For example, the $[Mo^VMo^{VI}O_{19}]^{3-}$ species was shown to exhibit a 6-line hyperfine structure at 77 K, implying electron localization on one molybdenum atom only, in the ESR time scale.[10] In the case of $[PMo^VMo_{11}{}^{VI}O_{40}]^{4-}$, a puzzling result was first obtained: a six-line hyperfine structure appeared below 60 K, but the whole spectrum remained isotropic, which would have implied the mobility of the electron at this temperature.[1c,2] We have shown later that the spectrum was actually anisotropic, a result fully consistent with electron trapping.[15]

Herein we report the results for several one-electron-reduced species of the Keggin type α-$[XMo^VMo^{VI}{}_{11}O_{40}]^{n-}$ (X = Si, Ge, P, As) and show the generality of the behavior observed in the case of $[PMo_{12}O_{40}]^{4-}$. The comparison is made with $[Mo_6O_{19}]^{3-}$ or β-$[SiMo_3W_9O_{40}]^{5-}$ and "trapped systems" such as $[Mo^VW^{VI}{}_5O_{19}]^{3-}$ and α-$[SiMo^VW_{11}O_{40}]^{5-}$. The latter compounds can be used as references in which no homonuclear electron transfer process can take place. For some typical homonuclear systems such as $[PMo_{12}O_{40}]^{4-}$ or $[GeMo_{12}O_{40}]^{5-}$, a complete computer simulation of the spectrum over a wide temperature range has provided the rate of thermal electron transfer and the corresponding activation energy. There are only few examples so far of such determinations for nonextended mixed-valence systems.[16] These values have been compared with the E_{op} values in order to evaluate the importance of the electronic interaction. Finally, the relationships between ground-state delocalization, thermal activation energy, and structural parameters are discussed.

Structural Considerations. The studied compounds have either the Lindqvist[17] M_6O_{19} structure or the Keggin[18] (α) $XM_{12}O_{40}$ structure. The Lindqvist structure (Figure 1) is made of six MO_6 octahedra sharing edges and having a common vertex. The resulting structure exhibits an octahedral symmetry. The Keggin structure (Figure 2) is made of four M_3O_{13} groups in a tetrahedral arrangement around the X heteroatom. In each M_3O_{13} group, the MO_6 octahedra are linked by edge-sharing, as in M_6O_{19}, while the MO_6 octahedra belonging to different M_3O_{13} groups are sharing corners. The so-called β structure[19] of β-$[SiW_9Mo_3O_{40}]^{4-}$ derives from the Keggin structure by rotating one M_3O_{13} group by 60° around a ternary axis (Figure 3). This compound is included in the present study because the structure of the related defect heteropolyanion β-$[SiW_9O_{34}H]^{9-}$ has been recently solved.[20] It shows that the three missing tungsten atoms are taken from different W_3O_{13} groups. This result invalidates the earlier assumption[21] that a complete W_3O_{13} group was missing. Since β-$[SiMo_3W_9O_{40}]^{4-}$ is prepared from β-$[SiW_9O_{34}H]^{9-}$, it seems reasonable to assume that the three molybdenum atoms of β-$[SiMo_3W_9O_{40}]^{4-}$ belong to three different M_3O_{13} groups.[22] Thus they should be linked by corner sharing, as shown in Figure 3.

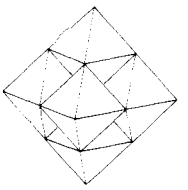

Figure 1. The Lindqvist M_6O_{19} structure.

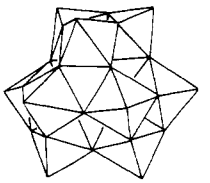

Figure 2. The Keggin (α) $XM_{12}O_{40}$ structure. Only three M_3O_{13} groups have been represented, for clarity.

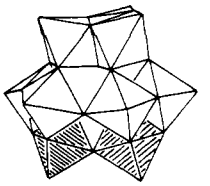

Figure 3. The β-$XM_{12}O_{40}$ structure. The upper M_3O_{13} group has been rotated with respect to the Keggin structure. In β-$[SiMo_3W_9O_{40}]^{4-}$ the three MoO_6 octahedra occupy the shaded positions.

Experimental Section

In order to avoid hydrolytic reactions and to ensure the stability of one-electron-reduced forms, all experiments were performed with tetrabutylammonium salts dissolved in dimethylformamide.

Preparation of Nonreduced Compounds. $(NBu_4)_2[Mo_6O_{19}]$. The method has been already described.[10]

α-$(NBu_4)_4[SiMo_{12}O_{40}]$. The following modification of Copaux's method[23] was used: 37 mL of concentrated (13 M) HNO_3 was added to 120 mL of a Na_2MoO_4 (1 M) solution. Then 50 mL of a metasilicate solution (0.2 M) was added dropwise; the resulting solution turned yellow. After 30 min at 80 °C during which the $\beta \rightarrow \alpha$ isomerization took place, the precipitation was performed by adding 12 g of NBu_4Br in 10 mL of water. The precipitate was filtered and washed with water, ethanol, and ether. Recrystallization in acetone yielded 20 g of product as small yellow needles; IR (cm^{-1}, * = cation band) 985 (w), 945 (sh), 940 (s), 899 (vs), 868* (sh), 795 (vs), 735* (sh), 635 (w), 600 (sh), 532 (w), 509 (w), 463 (m), 452 (w), 397 (sh), 380 (s), 340 (m).

α-$(NBu_4)_4[GeMo_{12}O_{40}]$. The same procedure was used with 40 mL of HNO_3 (13 M), 120 mL of Na_2MoO_4 (1 M) and 27 mL of a solution of Na_2GeO_3 (0.38 M) in 0.52 M NaOH. Recrystallization in acetone yielded 20 g of product as small yellow crystals; IR (cm^{-1}, * = cation band) 960 (sh), 939 (s), 880 (sh), 873 (vs), 812 (vs), 778 (vs), 735* (sh), 635 (w), 605 (sh), 507 (m), 465 (m), 449 (m), 377 (s), 360 (sh), 330 (m).

α-$(NBu_4)_3[PMo_{12}O_{40}]$. The classical preparation[24] was improved by

(5) This results from the so-called PKS treatment of a 2-center mixed-valence system: Wong, K. Y.; Schatz, P. N.; Piepho, S. B. *J. Am. Chem. Soc.* **1979**, *101*, 2793. E_{op} equals the quantity $2\lambda^2$ of the PKS model in all the localized range. This equation is also given by: Cannon, R. "Electron Transfer Reactions"; Butterworths: London, 1980; p 274.

(6) Rabette, P.; Ropars, C.; Grivet, J. P. *C. R. Hebd. Seances Acad. Sci., Ser. C* **1967**, *265*, 153.

(7) Kazanskii, L. P. *Izv. Akad. Nauk SSSR, Ser. Khim.* **1978**, *2*, 274.

(8) Zaitov, M. M. *Russ. J. Inorg. Chem. (Engl. Transl.)* **1975**, *20*, 1726. Zaitov, M. M. *Zh. Strukt. Khim.* **1975**, *16*, 391.

(9) Potapova, I. V.; Karpukhina, T. A.; Kazanskii, L. P.; Spitsyn, V. I. *Izv. Akad. Nauk SSSR, Ser. Khim.* **1979**, *4*, 724.

(10) Che, M.; Fournier, M.; Launay, J. P. *J. Chem. Phys.* **1979**, *71*, 1954.

(11) Otake, M.; Komiyama, Y.; Otaki, T. *J. Phys. Chem.* **1973**, *77*, 2896.

(12) Maksimovskaya, R. I.; Kuznetsova, L. I.; Matveev, K. I. *Koord. Khim.* **1977**, *3*, 685.

(13) Spitsyn, V. I.; Potapova, I. V.; Kazanskii, L. P. *Dokl. Akad. Nauk SSSR* **1978**, *243*, 426.

(14) Dorokhova, E. N.; Kazanskii, L. P. *Dokl. Akad. Nauk SSSR* **1976**, *229*, 622.

(15) Launay, J. P.; Fournier, M.; Sanchez, C.; Livage, J.; Pope, M. T. *Inorg. Nucl. Chem. Lett.* **1980**, *16*, 257.

(16) Recent examples of electron transfer rate determination are a flash photolysis experiment (Creutz, C.; Kroger, P.; Matsubara, T.; Netzel, T. L.; Sutin, N. *J. Am. Chem. Soc.* **1979**, *101*, 5442) and a Mossbauer study over a wide range of temperatures (Dziobkowski, C. T.; Wrobleski, J. T.; Brown, D. B. *Inorg. Chem.* **1981**, *20*, 679).

(17) Lindqvist, I. *Ark. Kemi* **1953**, *5*, 247; **1955**, *7*, 49.

(18) Keggin, J. F. *Proc. R. Soc. London, Ser. A* **1934**, *A144*, 75.

(19) Matsumoto, K. Y.; Kobayashi, A.; Sasaki, Y. *Bull. Chem. Soc. Jpn.* **1975**, *48*, 3146.

(20) Robert, F.; Tézé, A. *Acta Crystallogr., Sect. B* **1981**, *37*, 318. See also: Hervé et al. (Hervé, G.; Tézé, A.; Leyrie, M. *J. Coord. Chem.* **1979**, *9*, 245) for the implications of this structural result.

(21) Hervé, G.; Tézé, A. *Inorg. Chem.* **1977**, *16*, 2115.

(22) A structural rearrangement upon addition of molybdenum seems unlikely, since infrared spectroscopy shows that the β structure is retained in the reaction.

(23) Copaux, H. *Ann. Chim. (Paris)* **1906**, *7*, 118.

(24) Copaux, H. *Bull. Soc. Chim. Fr.* **1922**, *31*, 97.

using a low dielectric constant medium, i.e., a water–dioxane mixture H_3PO_4 (10 mL) (1 M) was added to a mixture of 120 mL of Na_2MoO_4 (1 M), 18 mL of HNO_3 (13 M), and 100 mL of 1,4-dioxane. The resulting yellow solution was precipitated by adding 10 g of NBu_4Br in 10 mL of water. After filtration, the yellowish solid was treated by 100 mL of boiling water, filtered again, and washed with water, ethanol, and ether. A yellow powder (20 g) was obtained and recrystallized in acetone; IR (cm^{-1}, * = cation band) 1063 (s), 1030* (vw), 965 (sh), 955 (vs), 880 (s), 805 (vs), 738* (vw), 612 (w), 505 (m), 464 (w), 386 (s), 340 (m).

α-$(NBu_4)_3[AsMo_{12}O_{40}]$. The preparation was performed according to a modification of Contant's procedure.[25] Solid MoO_3 (72 g), 6.3 g of As_2O_5, and 13.2 g of solid $LiOH·H_2O$ were mixed together and treated by 200 mL of hot water. The resulting solution (pH ~5) was concentrated to 80 mL and 100 mL of 1,4-dioxane was added, followed by 25 mL of concentrated (12 M) HCl. The solution turned orange-yellow and after a few minutes began to precipitate. After a few hours, it was filtered and the solid was washed with dioxane and ether, giving 70 g of a crude lithium salt as a yellow powder. The purity was checked by polarography on a glassy carbon electrode in a 0.5 M HCl–50% dioxane medium (five waves at +0.360, +0.245, +0.020, −0.130, and −0.230 V vs. SCE).

The lithium salt (70 g) was then dissolved in a mixture of 100 mL of 1,4-dioxane and 100 mL of water and precipitated by 30 g NBu_4Br dissolved in 50 mL dioxane. The resulting yellow salt (60 g) was dissolved in CH_3CN and reprecipitated by ether; IR (cm^{-1}, * = cation band) 980 (sh), 965 (s), 895 (vs), 855 (m), 790 (vs), 740* (vw), 608 (w), 498 (m), 470 (m), 453 (m), 379 (s), 330 (w).

α-$(NBu_4)_4[SiMoW_{11}O_{40}]$. Na_2MoO_4 (10 mL) (1 M) was added dropwise to 6 mL of HNO_3 (13 M). Then 10 g of $K_8[SiW_{11}O_{39}]·12H_2O$ (prepared according to ref 26) was dissolved by small fractions. The potassium salt of molybdotungstosilicate precipitated as a yellow solid. After a few hours, it was filtered and washed with a saturated KCl solution, ethanol, and ether. Recrystallization was performed by dissolving the filtrate in water at room temperature, filtering a small amount of a white solid ($K_8SiW_{11}O_{39}$), and allowing it to stand at 0 °C. Beautiful yellow needles were obtained after 1 day. The purity of this salt ($K_4[SiMoW_{11}O_{40}]·16H_2O$) was checked by polarography in a monochloracetate buffer pH 2.7 (three waves at +0.25, −0.42, −0.77 V vs. SCE).[27] Then 10 g of this salt was dissolved in 30 mL of water and precipitated by 10 g of NBu_4Br. The resulting yellow salt was washed with water, ethanol, and ether; IR (cm^{-1}, * = cation band); 1009 (m), 985 (sh), 967 (s), 918 (s), 881 (s), 793 (vs), 735* (sh), 545 (sh), 530 (m), 478 (vw), 415 (vw), 384 (s), 335 (m).

β-$(NBu_4)_4[SiMo_3W_9O_{40}]$. A Na_2MoO_4 (40 mL) solution (1 M) was acidified by 60 mL of 12 M HCl. Then 27 g of β-$Na_9(HSiW_9O_{34})·23H_2O$ (prepared according to ref 21) was slowly added. After 30 min, the resulting pale yellow solution was precipitated by solid KCl. The potassium salt of 3-molybdo-9-tungstosilicate was filtered and washed with a saturated KCl solution, ethanol, and ether. A yellow product (25 g) was collected. The purity was checked by polarography in 0.1 M $HClO_4$–0.9 M $NaClO_4$ on a glassy carbon rotating electrode (four waves at +0.380, +0.160, −0.220, and −0.450 V vs. SCE[27]). This crude product (25 g) was then dissolved in 50 mL of water and precipitated by 20 g of NBu_4Br dissolved in 20 mL of water. The yellow tetrabutylammonium salt was filtered, washed with water, ethanol, and ether, and recrystallized in acetone; IR (cm^{-1}, * = cation band) 1005 (w), 983 (sh), 967 (sh), 960 (s), 910 (vs), 875* (sh), 865* (sh), 810 (vs), 794 (sh), 740* (sh), 610 (w), 543 (sh), 530 (m), 515 (m) 465 (sh), 421 (w), 400 (w), 381 (sh), 376 (m), 361 (w), 340 (m). The acid $H_4[SiMo_3W_9O_{40}]·30H_2O$ was also prepared, by dissolving the crude potassium salt in water and extraction by ether and HCl.

Compounds Prepared in the Reduced Form. $(NBu_4)_3[MoW_5O_{19}]$. The preparation required the reaction of a reactive form of $WO_3·H_2O$ upon MoO_4^{2-}. $Na_2WO_4·2H_2O$ (150 g) was dissolved in 250 mL of water and precipitated at 100 °C by a solution of 75 g of $CaCl_2·2H_2O$ in 100 mL of water. The resulting $CaWO_4$ was washed several times by decantation and poured into 1 L of 2 M HCl at 70 °C under vigorous stirring. A yellow precipitate of $WO_3·H_2O$ appeared which was washed several times by decantation until complete elimination of chloride. It was then poured slowly into 50 mL of 1 M Na_2MO_4 at 80 °C. The first fractions were rapidly digested, but near the end of the addition, the solution remained cloudy. Then solid Na_2CO_3 was simultaneously added in order to keep the pH above 6. Finally, when all the $WO_3·H_2O$ was added, the pH was adjusted to 7–8 and the mixture boiled for 30 min. After the solution was cooled, it was filtered, diluted to 200 mL, and precipitated with 45 g of NBu_4Br. The heterogeneous mixture was heated to 90 °C for 30 min before filtration. The precipitate was washed with boiling water and air-dried. Recrystallization in acetone yielded pale yellow crystals. At this stage, polarographic and Raman studies revealed that the crystals were composed mainly of $(NBu_4)_2[W_6O_{19}]$ (~80%) and $(NBu_4)_2[MoW_5O_{19}]$ (~20%). An electrochemical reduction was necessary to eliminate the unwanted hexatungstate salt. The recrystallized product (14 g) was dissolved in 70 mL of DMF containing 0.4 M NBu_4BF_4 as supporting electrolyte. The solution was electrolyzed at −0.5 V vs. SCE: only $[MoW_5O_{19}]^{2-}$ was reduced at this potential. The resulting blue solution was evaporated under vacuum with a liquid nitrogen trap. After several days, blue crystals of the reduced product $(NBu_4)_3[MoW_5O_{19}]$ began to appear. It happened sometimes that the unreduced $(NBu_4)_2[W_6O_{19}]$ also crystallized, but as colorless crystals that were easily separated by hand picking. Finally the blue crystals were washed with acetone. Polarography in DMF containing NBu_4BF_4 showed that the main product was $(NBu_4)_3[MoW_5O_{19}]$ (anodic wave at −0.30 V and cathodic wave at −1.90 V) with about 7% of $(NBu_4)_3[Mo_2W_4O_{19}]$ (characteristic wave at −1.32 V). Anal. $(NBu_4)_3[MoW_5O_{19}]$: C, H, N; W:Mo ratio: calcd 5.00; found 4.80. IR (cm^{-1}, * = cation band) 978 (sh), 953 (vs), 884 (m), 798 (vs), 790 (sh), 735* (sh), 608 (sh), 583 (m), 573 (sh), 444 (s), 433 (s), 368 (vw), 352 (w).

β-$H(NBu_4)_4[SiMo_3W_9O_{40}]$. An aqueous solution of β-$H_4[SiMo_3W_9O_{40}]·30H_2O$ (3.16 g in 100 mL of 1 M $HClO_4$) was electrolyzed at +0.3 V on a platinum electrode and precipitated by NBu_4Br. Small blue crystals were obtained after recrystallization in acetone. Analysis yielded the composition $H(NBu_4)_4[SiMo_3W_9O_{40}]$; IR ($cm^{-1}$ * = cation band) 1003 (w), 985 (sh), 967 (sh), 960 (s), 910 (vs), 870* (sh), 810 (vs), 791 (sh), 740* (sh), 620 (vw), 580 (w), 546 (w), 535 (w), 470 (vw), 421 (vw), 401 (m), 383 (sh), 375 (m), 362 (sh), 340 (m).

Electrochemical Reductions. The electrochemical reductions were carried out on a mercury or platinum cathode in DMF containing 0.2–0.5 mol L^{-1} NBu_4BF_4 as supporting electrolyte. The potential was imposed by a Tacussel PRT 20-2 potentiostat with respect to an aqueous saturated calomel electrode. The progress of the reduction to the one-electron stage was followed by coulometry (using a Tacussel IG4-1100 integrator), potentiometry, and polarography. The polyanion concentration was generally 10^{-2} M.

Preparation of Solutions for ESR Experiments. For most compounds, the ESR was carried out directly on the electrolyzed solution. In the case of $[MoW_5O_{19}]^{3-}$, a solution of the reduced salt in DMF was prepared. For β-$[SiMo_3W_9O_{40}]^{5-}$, it was concluded from a detailed UV–vis spectroscopic study that the electrolysis method yielded a partially protonated product. The best ESR results were obtained with a solution of the acid salt β-$H(NBu_4)_4[SiMo_3W_9O_{40}]$ to which 1 equiv of NBu_4OH had been added. This solution exhibited a visible–near-infrared spectrum in agreement with the one given in ref 28.

Electronic and IR Spectra. Electronic spectra were recorded with a Beckman 5240 UV–visible–near-infrared spectrophotometer between 2000 and 400 nm; Infrared spectra were recorded between 1100 and 300 cm^{-1} in KBr pellets.

ESR Spectra. X-band ESR spectra were recorded on a Jeol ME 3X spectrometer equipped with an Oxford Instrument cryostat in order to perform low-temperature experiments down to 4 K. Magnetic field was measured with an NMR proton probe and the microwave frequency with a wavemeter giving an accuracy of ±1 MHz.

Results

Electron Spin Resonance. $[MoW_5O_{19}]^{3-}$. The ESR spectra of a solution in DMF are given in Figure 4. The room temperature spectrum (Figure 4a) is typical of a Mo^{5+} ion. The strong central line is related to the75% abundant ^{96}Mo isotope, while the weak hyperfine lines are due to the two other ^{95}Mo and ^{97}Mo isotopes having a nuclear spin $I = {}^5/_2$.[29] The ESR spectrum can be described by the classical isotropic Hamiltonian, $H_{iso} = g_{iso}\beta HS + A_{iso}(SI)$, with $g_{iso} = 1.921$ and $A_{iso} = 55$ G.

The frozen solution spectrum (Figure 4b) exhibits the parallel and perpendicular features typical of a Mo^{5+} ion in an axial ligand field. It can be described by the following spin Hamiltonian:

$$H = g_{\parallel}\beta H_z S_z + g_{\perp}\beta(H_x S_x + H_y S_y) + A_{\parallel} S_z I_z + A_{\perp}(S_x I_x + S_y I_y)$$

(25) Contant, R.; Souchay, P. *C. R. Hebd. Seances Acad. Sci., Ser. C* **1967**, *265*, 723.
(26) Tězě, A.; Hervé, G. *J. Inorg. Nucl. Chem.* **1977**, *39*, 999.
(27) Contant, R.; Fruchart, J. M.; Hervé, G.; Tězě, A. *C. R. Ser. Hebd. Seances Acad. Sci., Ser. C* **1974**, *278*, 199.
(28) Fruchart, J. M.; Hervé, G.; Launay, J. P.; Massart, R. *J. Inorg. Nucl. Chem.* **1976**, *38*, 1627.
(29) These two isotopes have almost the same nuclear magnetic moment and cannot therefore be distinguished on the spectrum.

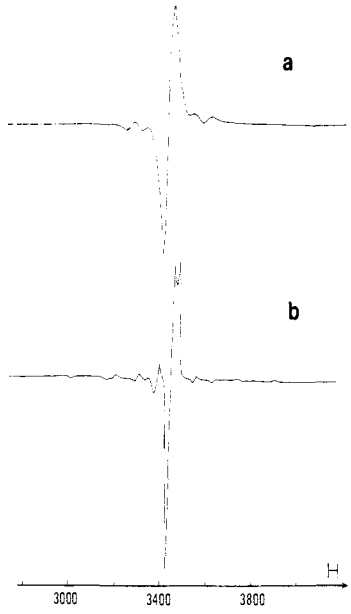

Figure 4. ESR spectra of $[MoW_5O_{19}]^{3-}$; a = room temperature; b = 10 K (frozen solution).

Table I. Anisotropic ESR Parameters of the One-Electron-Reduced Species[a]

compound	$g_\parallel(g_z)$	$g_\perp(g_x,g_y)$	$A_\parallel$	$A_\perp$
$[MoW_5O_{19}]^{3-}$	1.917	1.924	85.2	39.7
$[Mo_6O_{19}]^{3-}$	1.916	1.930	80.5	33.5
α-$[SiMoW_{11}O_{40}]^{5-}$	1.914	1.931	82.5	35.6
α-$[PMo_{12}O_{40}]^{4-}$	1.938	1.949	60.7	27.2
α-$[AsMo_{12}O_{40}]^{4-}$	1.935	1.948	64.4	28.2
α-$[SiMo_{12}O_{40}]^{5-}$	1.931	1.944	65.5	32.0
α-$[GeMo_{12}O_{40}]^{5-}$	1.935	1.951	68.5	33.6
β-$[SiMo_3W_9O_{40}]^{5-}$	1.921	1.950, 1.935	63.5	30.8

[a] Hyperfine coupling constants in gauss. [b] Orthorhombic spectrum.

The main axis of both axially symmetric g and A tensors have been taken along the distorsion axis z, i.e., the direction of the Mo=O shortest bond. ESR parameters have been detemined by computer simulation. The best fit between simulated and experimental spectra was obtained for the values reported on Table I.

The ESR line width does not vary in the 4–200-K temperature range, showing that the unpaired electron remains localized on the molybdenum site. Above 220 K, the solution is no longer frozen and the molecular tumbling leads to an isotropic spectrum.

$[Mo_6O_{19}]^{3-}$. The ESR spectrum has already been described in a previous paper.[10] The room temperature solution spectrum exhibits a single line only, without any resolved hyperfine structure (Figure 5a). Hyperfine lines can be observed at low temperature (Figure 5b). The spectrum in Figure 5 is typical of a Mo^{5+} ion in axial symmetry and can be described with the same spin Hamiltonian as for $[MoW_5O_{19}]^{3-}$. The ESR parameters determined by computer simulation are reported in Table I. An example of simulated spectrum is given in Figure 5c. The frozen solution spectrum remains well resolved up to 110 K. It then begins to broaden, and the hyperfine structure disappears above 117 K. The line broadening increases with temperature and a purely Lorentzian line shape is observed above 200 K. A computer simulation analysis of the experimental line shape and line width has been performed in a temperature range up to 400 K, using a powder spectrum in order to avoid molecular tumbling. A plot of the peak to peak half-width, $^1/_2\Delta H_{pp}$, vs. temperature is shown in Figure 9.

α-$[SiMoW_{11}O_{40}]^{5-}$. The ESR spectra in DMF exhibit a well-resolved hyperfine structure at room temperature as well as in the frozen state (Figure 6). The line width does not vary with temperature, and the frozen solution spectrum can be described by an axial spin Hamiltonian. The ESR parameters are reported in Table I.

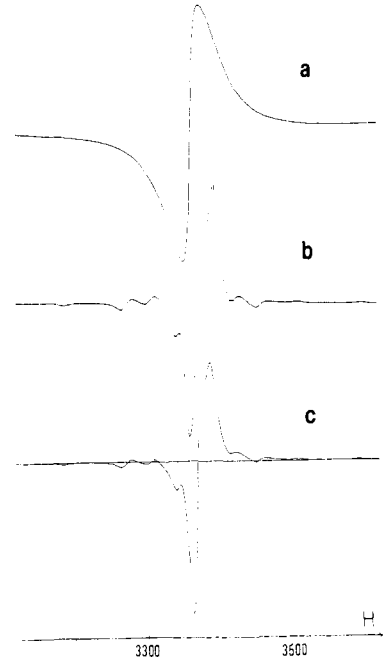

Figure 5. ESR spectra of $[Mo_6O_{19}]^{3-}$; a = room temperature; b = 10 K (frozen solution); c = simulated 10 K spectrum.

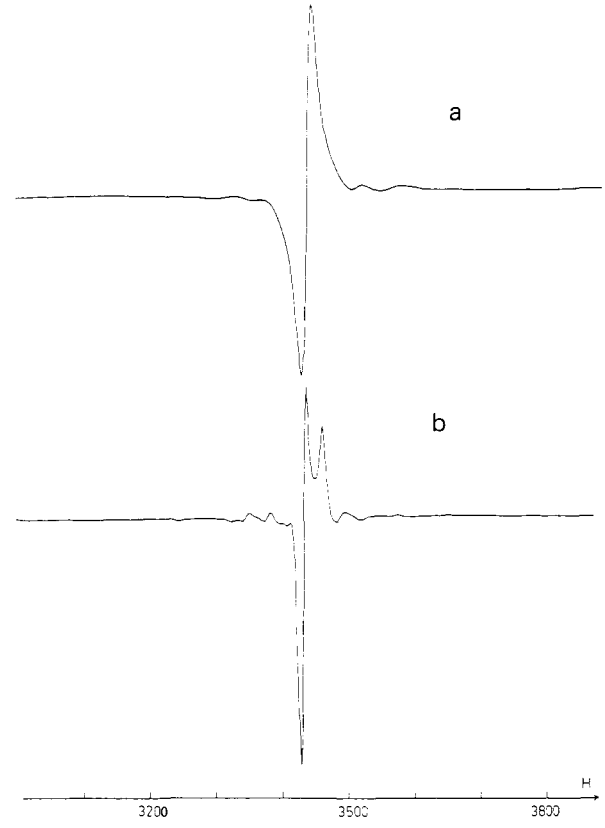

Figure 6. ESR spectra of α-$[SiMoW_{11}O_{40}]^{5-}$; a = room temperature; b = 77 K (frozen solution).

α-$[XMo_{12}O_{40}]^{n-}$ (X = P, As, Si, Ge). The frozen solution spectra recorded near 10 K (Figure 7a) are typical of unpaired electrons trapped on a single molybdenum atom in an axially distorted ligand field (Table I). The hyperfine structure remains well resolved up to 40 K; above this temperature, a line broadening is observed and all hyperfine components disappear above 45 K (Figures 7b and 7c). A computer simulation of the line width and line shape has been performed as previously (Figure 8). A plot of the peak

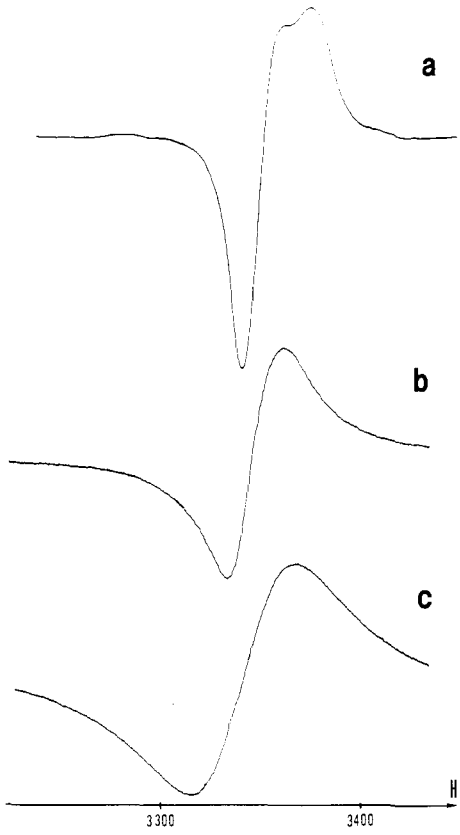

Figure 7. Evolution of the central line shape of $[GeMo_{12}O_{40}]^{5-}$ with temperature; a = 10 K; b = 70 K; c = 140 K.

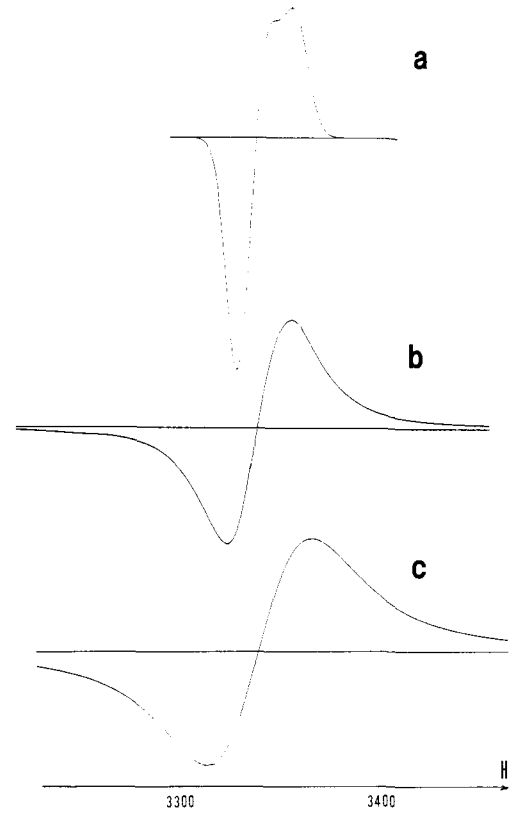

Figure 8. Same as Figure 7, but simulated spectra.

to peak half-width, $^1/_2\Delta H_{pp}$, vs. temperature, is reported in Figure 9 for $[PMo_{12}O_{40}]^{4-}$ and $[GeMo_{12}O_{40}]^{5-}$.

β-$[SiMo_3W_9O_{40}]^{5-}$. The frozen solution spectrum is orthorhombic and can be described by the following spin Hamiltonian:

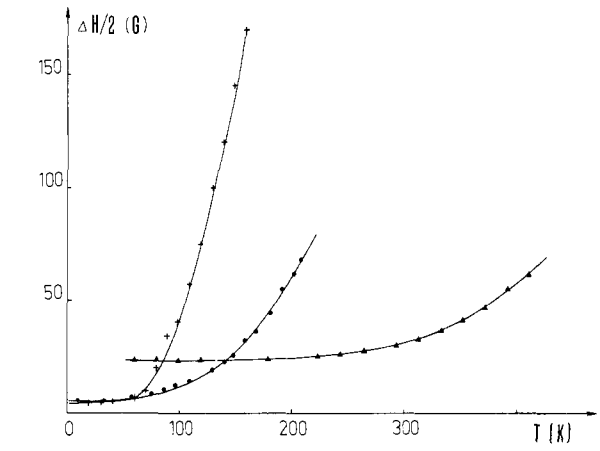

Figure 9. Simulated half-width $^1/_2\ \Delta H_{pp}$ as a function of temperature; (▲) $[Mo_6O_{19}]^{3-}$; (●) $[GeMo_{12}O_{40}]^{5-}$; (+) $[PMo_{12}O_{40}]^{4-}$.

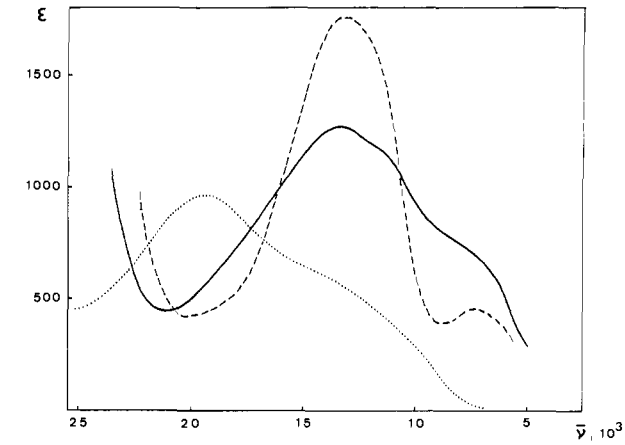

Figure 10. Visible–near-infrared spectra of α-$[SiMo_{12}O_{40}]^{5-}$ (—), α-$[SiMoW_{11}O_{40}]^{5-}$ (····), and β-$[SiMo_3W_9O_{40}]^{5-}$ (- - - -).

Table II. Electronic Spectra[a]

compound	band positions[a]		
$[MoW_5O_{19}]^{3-}$	16 700 (155)	11 300 sh	
$[Mo_6O_{19}]^{3-}$	20 400 (340)	11 600 (175)	9000 sh
α-$[SiMoW_{11}O_{40}]^{5-}$	19 600 (950)	13 000 sh	
α-$[PMo_{12}O_{40}]^{4-}$	18 500 sh	13 150 (1600), 11 600 sh	8600 sh, 6400 sh[b]
α-$[AsMo_{12}O_{40}]^{4-}$		13 050 (1000), 11 900 sh	
α-$[SiMo_{12}O_{40}]^{5-}$	18 500 sh	13 300 (1270), 11 500 sh	7000 sh
α-$[GeMo_{12}O_{40}]^{5-}$		13 700 (1160), 11 600 sh	7300 sh
β-$[SiMo_3W_9O_{40}]^{5-}$		13 200 (1750), 11 700 sh	7300 (450)

[a] Band positions in cm^{-1}; molar extinction coefficients in parentheses; sh = shoulder. [b] Very weak shoulder.

$$H = g_z\beta H_z S_z + g_x\beta H_x S_x + g_y\beta H_y S_y + A_z S_z I_z + A_x S_x I_x + A_y S_y I_y$$

The corresponding ESR parameters, determined by computer simulation, are reported in Table I. The A_x and A_y components are not resolved enough to be separated. The spectrum begins to broaden around 55 K and the hyperfine structure disappears above 60 K.

Electronic Spectra. Band positions and intensities are reported in Table II. The spectra of $[SiMo_{12}O_{40}]^{5-}$, $[SiMoW_{11}O_{40}]^{5-}$, and β-$[SiW_9Mo_3O_{40}]^{5-}$ are represented in Figure 10. Spectra of $[Mo_6O_{19}]^{3-}$ and $[MoW_5O_{19}]^{3-}$ can be found in ref 30. The four

(30) Jeannin, Y.; Launay, J. P.; Sanchez, C.; Livage, J.; Fournier, M. *Nouv. J. Chim.* **1980**, *4*, 587.

heterododecamolybdates display analogous spectra with generally three bands as in the case of dodecatungstates.[28,31] The band near 12000 cm^{-1} has an asymmetrical shape and seems to contain two components, i.e., a maximum near 13000 cm^{-1} and a shoulder near 11000 cm^{-1}. The weak shoulder near 18500 cm^{-1} is unambigously observed only for $[PMo_{12}O_{40}]^{4-}$ and $[SiMo_{12}O_{40}]^{5-}$.

Discussion

Low-Temperature ESR Results: Valence Trapping and Ground-State Delocalization. ESR spectra of one-electron-reduced polyanions show that the unpaired electron becomes trapped on a single molybdenum atom at low enough temperatures. This is clearly demonstrated by the occurrence of a six-line anisotropic hyperfine structure.[15] From the low-temperature spectra, it is thus possible to get information about the ligand field around Mo^{5+} ions and the degree of delocalization in the ground state.

According to structural data, molybdenum is surrounded by six oxygen atoms in both Lindqvist and Keggin structures with a site symmetry close to C_{4v}.[32] The distortion axis (z) lies along the shortest Mo=O double bond (Mo–O ~1.7 Å). Four oxygens lie in the xy plane (Mo–O ~1.9 Å), and the sixth oxygen is much farther apart (Mo–O ~2.3 Å), below the equatorial plane. The molybdenum atom is found ca. 0.35 Å above the equatorial xy plane in the direction of the unshared outermost oxygen.

The ESR results are consistent with a ligand field around Mo^{5+} that is only axially distorted and can be approximated to C_{4v}.[33] Since the true site symmetry in nonreduced Keggin polyanions is only C_s, this suggests that Mo^{5+} ions do not occupy exactly the same position as Mo^{6+} ions. They are presumably slightly shifted toward the center of the octahedron in such a way that the four equatorial oxygens become nearly equivalent from an ESR point of view. This would be in agreement with the known tendency for Mo^{5+} to adopt more symmetrical environments than Mo^{6+}.[34] This shift has also been recently observed for vanadium mixed-valence compounds.[35] Only β-$[SiMo_3W_9O_{40}]^{5-}$ gave an orthorhombic spectrum. This seems to be characteristic of the β structure: recent ESR results have shown that all MoO_6 octahedra are much more distorted in the β isomers than in the α isomers.[36] It can be noticed that the behavior of molybdenum contrasts with the tungsten for which orthorhombic spectra are systematically observed even for the α (Keggin) series.[2] This is attributed to the higher spin–orbit coupling constant for tungsten, leading to a larger spread in g values.

The ESR spectra being easily observed at room temperature, this means that the unpaired electron is in an orbitally nondegenerate ground state, i.e., in a b_2 (d_{xy}) orbital. The ground-state wave function can then be expressed as

$$|b_2\rangle = \beta|d_{xy}\rangle - \beta'|\Psi_{b_2}\rangle$$

where $|\Psi b_2\rangle$ represents the oxygen 2p orbital combination having b_2 symmetry. The mixing coefficient β can be determined from the hyperfine coupling parameters by[37]

$$A_\parallel = P[-{}^4/_7\beta^2 - K\beta^2 + g_\parallel - 2.0023 + {}^3/_7(g_\perp - 2.0023)]$$

$$A_\perp = P[{}^2/_7\beta^2 - K\beta^2 + {}^{11}/_{14}(g_\perp - 2.0023)]$$

where K is the isotropic Fermi contact term and $P = 2.0023 g_n\beta_e\beta_n\langle r^{-3}\rangle$. P depends on the effective charge carried by the molybdenum atom. The P value referring to Mo^{3+} is usually taken, i.e., -55.10^{-4} cm^{-1}, according to McGarvey.[38] Thus β and K can be obtained from the measured $A_\parallel$ and $A_\perp$ values (see Table III where we have included the results for $(PMoW_{11}O_{40})^{4-}$[39]).

Table III. Ground-State Delocalization Coefficients (β) and Fermi Contact Terms (K)

compound	β	K
$[MoW_5O_{19}]^{3-}$	0.90	0.82
$[Mo_6O_{19}]^{3-}$	0.90	0.74
α-$[PMoW_{11}O_{40}]^{4-}$ [a]	0.84	0.76
α-$[SiMoW_{11}O_{40}]^{5-}$	0.90	0.76
α-$[PMo_{12}O_{40}]^{4-}$	0.77	0.58
α-$[AsMo_{12}O_{40}]^{4-}$	0.78	0.60
α-$[SiMo_{12}O_{40}]^{5-}$	0.77	0.65
α-$[GeMo_{12}O_{40}]^{5-}$	0.79	0.69
β-$[SiMo_3W_9O_{40}]^{5-}$	0.79	0.62

[a] Values from the ESR parameters given in ref[39].

Inspection of Table III shows that β is close to 0.9 in the Lindqvist structures, whereas it is generally smaller than 0.9 in the Keggin structures. In other respects, the β values and thus the degrees of ground-state delocalization are the same in $[MoW_5O_{19}]^{3-}$ and $[Mo_6O_{19}]^{3-}$. In $[MoW_5O_{19}]^{3-}$, the unpaired electron cannot be delocalized on the neighboring tungsten atoms because the tungsten orbitals are higher in energy than the molybdenum orbitals. Therefore, the ground-state delocalization in $[Mo_6O_{19}]^{3-}$ seems to be also restricted to the ligand oxygen atoms and not to involve the neighboring molybdenum atoms.

By contrast, in the Keggin series, β decreases markedly when going from "trapped systems" such as $[PMoW_{11}O_{40}]^{4-}$ or $[SiMoW_{11}O_{40}]^{5-}$ to genuine mixed-valence systems $[XMo_{12}O_{40}]^{n-}$, showing the effect of a more delocalized ground-state involving the neighboring molybdenum atoms. This is even more obvious if we compare the Fermi contact terms. This term arises from the spin polarization of inner "s" electrons by outer 4d unpaired electron and is thus very sensitive to the radial extension of the 4d electronic orbital. The lowest values are also obtained for the Keggin mixed-valence systems, which is consistent with a greater ground-state delocalization.

The nature of the central element of the Keggin structure (Si^{IV}, P^V, Ge^{IV}) appears to influence noticeably the measured values of K which range from 0.58 for $[PMo_{12}O_{40}]^{4-}$ to 0.69 for $[GeMo_{12}O_{40}]^{5-}$. This could be due to the electrostatic field created by the central element and its attraction on the unpaired electron. We shall see later that is also increases slightly the thermal energy for hopping from P to Ge.

Finally, it can be noticed that the g anisotropy decreases significantly when going from $[GeMo_{12}O_{40}]^{5-}$ ($g_\perp - g_\parallel = 0.016$) to $[PMo_{12}O_{40}]^{4-}$ ($g_\perp - g_\parallel = 0.011$). This difference is mainly due to a decrease of the $g_\parallel$ value. The unpaired electron lying in a b_2 (d_{xy}) orbital, the $g_\parallel$ value, is given by

$$g_\parallel = 2.0023 - \frac{8\lambda}{E_{b_1} - E_{b_2}}$$

(31) Varga, G. M.; Papaconstantinou, E.; Pope, M. T. *Inorg. Chem.* **1970**, *9*, 662.

(32) The following species have been studied by X-ray crystallography. $[Mo_6O_{19}]^{2-}$: Allcock, H. R.; Bissel, E. C.; Shawl, E. T. *Inorg. Chem.* **1973**, *12*, 2963. Garner, C. D.; Howlader, N. C.; Mabbs, F. E.; McPhail, A. T.; Miller, R. W.; Onan, K. D. *J. Chem. Soc., Dalton Trans.* **1978**, 1582. Nagano, O.; Sasaki, Y. *Acta Crystallogr., Sect. B* **1979**, *B35*, 2387. $[PMo_{12}O_{40}]^{3-}$: Strandberg, R. *Acta Chem. Scand., Ser. A* **1975**, *A29*, 359. Allmann, R. *Ibid.* **1976**, *A30*, 152. D'Amour, H.; Allmann, R. *Z. Kristallogr.* **1976**, *143*, 1. Boeyens, J. C. A.; McDougal, G. J.; Van R. Smit, J. *J. Solid State Chem.* **1976**, *18*, 191. Clark, C. J.; Hall, D. *Acta Crystallogr. Sect. B* **1976**, *B32*, 1545. $[SiMo_{12}O_{40}]^{4-}$: Ichida, H.; Kobayashi, A.; Sasaki, Y. *Ibid.* **1980**, *B36*, 1382. Fenst, M.; Molyanov, V. H.; Kazanskii, L. P.; Torchenkova, E. A.; Spitsyn, V. I. *Zh. Neorg. Khim.* **1980**, *25*, 733. $[GeMo_{12}O_{40}]^{4-}$: Strandberg, R. *Acta Crystallogr., Sect. B* **1977**, *B33*, 3090.

(33) Zaitov[8] has described a Q-band orthorhombic spectrum on a partially reduced crystal of $Ca_3[PMo_{12}O_{40}]_2 \cdot 58H_2O$. In our X-band experiments, the separation between g_x and g_y was too low, so that reliable simulation was only possible in axial symmetry.

(34) For example, Mo^{VI} oxo complexes are frequently of the MoO_2X_4 type, while Mo^V oxo complexes are of the more symmetrical $MoOX_5$ type. The structural chemistry of Mo^{VI} iso- and heteropolyanions shows distortions with respect to idealized structures, with an alternating pattern of long and short Mo–O bonds (see the discussion by: Garvey, J. F.; Pope, M. T. *Inorg. Chem.* **1978**, *17*, 1115).

(35) Hagenmuller, P. *Prog. Solid State Chem.* **1971**, *5*, 71.

(36) Sanchez, C.; Launay, J. P.; Fournier, M.; Livage, J., manuscript in preparation.

(37) De Armond, K.; Garrett, B. B.; Gutowsky, H. S. *J. Chem. Phys.* **1965**, *42*, 1019.

(38) McGarvey, B. R. *J. Phys. Chem.* **1967**, *71*, 51.

(39) Altenau, J. J.; Pope, M. T.; Prados, R. A.; So, H. *Inorg. Chem.* **1975**, *14*, 417.

where λ is the spin–orbit coupling constant. The optical transition energy, $E_{b_1} - E_{b_2}$, is about 18 500 cm^{-1} in $[PMo_{12}O_{40}]^{4-}$, where it appears as a weak shoulder on the edge of the intense 13 000-cm^{-1} band. This shoulder is no longer observed in $[GeMo_{12}O_{40}]^{5-}$, presumably because it has been red shifted and is hidden by the intense neighboring band. This suggests that the energy difference $E_{b_1} - E_{b_2}$ decreases from $[PMo_{12}O_{40}]^{4-}$ to $[GeMo_{12}O_{40}]^{5-}$, leading to a decrease of $g_{\parallel}$.

It thus appears that the central element can play a role in the structural properties of the polyanion. Such structural differences have been detected in the X-ray studies of nonreduced species.[32]

Thermal Electron Delocalization. The broadening of the ESR spectra with temperature indicates that thermal electron delocalization occurs when the paramagnetic Mo^{5+} ion is surrounded by other Mo^{6+} ions (Figure 9). This is due to electron hopping between metal sites. Such behavior is typical of class II mixed-valence compounds.

A detailed analysis of the line-shape and line-width variations with temperature can give information about this thermally activated hopping process. The measured peak to peak ESR line width $\Delta H_{pp(T)}$ increases with temperature and can be expressed as the sum of two terms:[40,41]

$$\Delta H_{pp(T)} = \Delta H_{pp(0)} + \delta H_{pp(T)}$$

The temperature-independent line width, $\Delta H_{pp(0)}$, is mainly due to dipolar interactions between paramagnetic ions together with nonresolved hyperfine couplings and ligand-field heterogeneities leading to a g value distribution. It corresponds to the line width at 0 K and can be obtained by extrapolation of the $\Delta H_{pp(T)} = f(T)$ plot (Figure 9).

The temperature-dependent line width, $\delta H_{pp(T)}$, is due to lifetime broadening caused by hopping motion induced spin relaxation.[41] An inhomogeneously broadened ESR absorption line $L(\omega - \omega_i)$ is made of spin packets $l(\omega - \omega_i)$ with width

$$1/T'_2 = (1/T_2) + (1/2T_1)$$

where T_1 and T_2 are respectively the spin–lattice and spin–spin relaxation times.

At very low temperatures, T_1 is rather long and the spin-packet line width, $1/T'_2$, is dominated by spin–spin interactions. T_1 decreases when the temperature is raised and when $1/2T_1$ becomes larger than $1/T_2$, the Lorentzian line width of a packet starts to depend on temperature. $\delta H_{pp(T)}$ then depends on the lifetime τ_s of the spin state. A detailed calculation has been performed by Movaghar and Schweitzer[40] showing that τ_s is proportional to the correlation time τ_h of the spin motion. Therefore we can write

$$\delta H_{pp(T)} = C\nu_h$$

where C is a proportionality factor and ν_h is the hopping frequency of the unpaired electron. According to Mott,[42] the hopping frequency can be expressed as

$$\nu_h = \nu_0 \exp(-2\alpha R) \exp(-E_{th}/kT)$$

where α is the rate of the wave function decay, R the distance between two molybdenum ions, and E_{th} the thermal activation energy for hopping. The first exponential corresponds to the tunneling effect and the second one to the thermally activated hopping. Thus E_{th} can be obtained from a plot of ln $\delta H_{pp(T)}$ vs. $1/T$ in the high temperature region where $1/2T_1$ is much larger than $1/T_2$. Such a plot is shown on Figure 11 for various mixed-valence polyanions and exhibits a linear behavior in the high-temperature limit as expected. The measured E_{th} are reported on Table IV. The preexponential term $\nu_0 \exp(-2\alpha R)$ is found to be about 10.[10] If ν_0 is taken as a phonon frequency ($\nu_0 \sim 10^{13}$ Hz), this would give $\exp(-2\alpha R) \sim 10^{-3}$. The distance R between adjacent molybdenum sites being about 3 Å, we can estimate the tunneling factor α to be about 1–1.3 $Å^{-1}$.

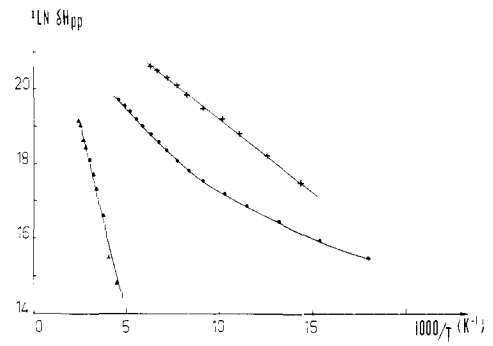

Figure 11. Ln δH_{pp} as a function of temperature. δH_{pp} is the temperature-dependent part of the line width. (▲) $[Mo_6O_{19}]^{3-}$; (●) $[GeMo_{12}O_{40}]^{5-}$; (+) $[PMo_{12}O_{40}]^{4-}$.

Table IV. Thermal Activation Energies, Optical Activation Energies, and Transfer Integrals (All in eV)[a]

compound	E_{th}	T_d	E_{op}[b]	J[c]	J[d]
$[Mo_6O_{19}]^{3-}$	0.155	117	1.125	0.15	
α-$[PMo_{12}O_{40}]^{4-}$	0.035	40	1.07	0.34	0.19 (0.33[e])
α-$[GeMo_{12}O_{40}]^{5-}$	0.045	50	0.913	0.25	0.26
β-$[SiMo_3W_9O_{40}]^{5-}$	0.055	~60	1.0	0.26	0.28

[a] T_d = Temperature for which the thermal delocalization begins to broaden the ESR spectrum (in K). [b] From the position of the lowest intervalence band. [c] Calculated from E_{th} and E_{op}, using eq 1. [d] Calculated from the optical spectrum, assuming that the separation between the two lowest energy bands is twice the resonance integral. [e] Calculated from the position of the very weak shoulder at 6400 cm^{-1} (see Table II).

Electronic Spectra. Owing to the very short time scale of UV–vis spectroscopy, the mobile electron appears trapped even at room temperature. Thus the crystal field (d–d) bands of Mo^{5+} centers are observed as well as the intervalence bands resulting from the optical excitation $Mo^{5+}\cdots O\cdots Mo^{6+} \rightarrow Mo^{6+}\cdots O\cdots Mo^{5+}$.

Starting with the Lindqvist type structures, we could assign the two bands at 11 600 cm^{-1} and 20 400 cm^{-1} in $[Mo_6O_{19}]^{3-}$ to the d–d transitions $^2B_2 \rightarrow {}^2E$ and $^2B_2 \rightarrow {}^2B_1$, respectively, *in* C_{4v} symmetry.[10] This assignment is at variance with the one proposed by Garner,[43] who states that the transition near 20 000 cm^{-1} in complexes containing the Mo^VO^{3+} unit is not a d–d transition but a charge-transfer transition. We think that this assignment does not hold for polyanions since this charge transfer transition (ligand → metal) would be expected to occur at a lower energy in the oxidized form, i.e., when Mo^V is replaced by Mo^{VI}, and actually no charge transfer transition is observed in $[Mo_6O_{19}]^{2-}$ below 31 000 cm^{-1}.

The shoulder near 9000 cm^{-1} in the spectrum of $[Mo_6O_{19}]^{3-}$ is assigned to an intervalence transition between edge-shared MoO_6 octahedra. This assignment is supported by the fact that no band is observed at this energy in $[MoW_5O_{19}]^{3-}$. The weak intensity of the intervalence transition would imply a weak electronic interaction between edge-shared MoO_6 octahedra in the $[Mo_6O_{19}]^{3-}$ structure.

The spectrum of $[MoW_5O_{19}]^{3-}$ exhibits only two bands which are assigned to d–d transitions. The molybdenum to tungsten intervalence transition is expected to be less intense than a molybdenum to molybdenum transition and to be blue shifted by about 5000 cm^{-1}.[44] Thus it should not be observed in the present spectrum. Curiously the $^2B_2 \rightarrow {}^2B_1$ occurs at a markedly lower energy (16 700 cm^{-1}) in $[MoW_5O_{19}]^{3-}$ with respect to $[Mo_6O_{19}]^{3-}$.

(40) Movaghar, B.; Schweitzer, L.; Overhof, H. *Philos. Mag.*, [*Part*] *B* **1978**, *37*, 683.
(41) Bachus, R.; Movaghar, B.; Schweitzer, L.; Voget-Grote, U. *Philos. Mag.*, [*Part*] *B* **1979**, *39*, 27.
(42) Austin, I. G.; Mott, N. F. *Adv. Phys.* **1969**, *18*, 41.
(43) Garner, C. D.; Hill, L. H.; Mabbs, F. E.; McFadden, D. L.; McPhail, A. T. *J. Chem. Soc., Dalton Trans.* **1977**, 853, and references therein.
(44) This value represents the difference in optical electronegativities between molybdenum and tungsten.[28] A similar value has been obtained by Diemann and Müller (Diemann, E.; Müller, A. *Chem. Phys. Lett.* **1974**, *27*, 351).

Since the energy of this transition is a measure of the equatorial ligand field strength, this would imply that the Mo_5O_{18} frame yields a stronger ligand field than that of W_5O_{18}. An analogous effect (although not so important) has been observed for substituted $[XZM_{11}O_{40}]$ polyanions.[45]

We now turn to the spectra of the four heterododecamolybdates and of β-$(SiMo_3W_9O_{40})^{5-}$. Let us begin with the low-energy side of the spectra (see Table II). All four $XMo_{12}O_{40}$ species exhibit shoulders near 7000–8000 cm^{-1}, which is outside the usual range for d–d transitions.[46] These features are thus assigned to intervalence transitions, an additional argument being the absence of absorption in this range for $[SiMoW_{11}O_{40}]^{5-}$. Since there are two kinds of junctions in the Keggin structure, namely the edge-sharing junctions between octahedra belonging to the same Mo_3O_{13} group and the corner-sharing junctions between octahedra belonging to different Mo_3O_{13} groups, one would expect two distinct intervalence transitions. It was thus proposed in 1976 that "intra-group" transitions occurred near 8000 cm^{-1} and "extra-group" transitions near 13 000 cm^{-1}.[28] However, this assignment was mainly based upon the observation of an intervalence band near 8000 cm^{-1} in α- and β-$[SiMo_3W_9O_{40}]^{5-}$ for which, at that time, the three molybdenum atoms were believed to belong the same M_3O_{13} group.[21] The present assumption about the structure of β-$[SiMo_3W_9O_{40}]^{5-}$ (three molybdenum atoms linked by corner sharing) is much more reliable, since it is based on a X-ray crystal structure determination.[20] Thus the 7300-cm^{-1} band observed in β-$[SiMo_3W_9O_{40}]^{5-}$ is clearly an "extra-group" transition, i.e., between corner-sharing octahedra.

Taking into account that the octahedra of a M_3O_{13} group are linked in the same way as in $[Mo_6O_{19}]^{3-}$, for which the intervalence transition is found near 9000 cm^{-1}, it now appears very likely that both "intra-group" and "extra-group" transition occur at roughly the same energy in heterododecamolybdates (7000–9000 cm^{-1})[47] so they would account for the shoulder in the near-infrared spectrum (see Table II).

We now consider the visible part of the spectra. All species exhibit a broad band near 12 000 cm^{-1}, partially resolved in two components, and in some cases a shoulder near 18 500 cm^{-1} (see Table II). This can be explained by the following two possibilities.

(i) These features might correspond to the d–d transitions $^2B_2 \rightarrow {}^2B_1$ (18 500 cm^{-1}) and $^2B_2 \rightarrow {}^2E$ (12 000 cm^{-1}). The splitting of the 12 000-cm^{-1} band would then be a consequence of the low-site symmetry of molybdenum removing the degeneracy of the ^2E level and the high intensity of these bands would be explained by the marked ground-state delocalization. However, a distortion leading to a splitting of the ^2E level of about 2000 cm^{-1} would give rise to an orthorombic ESR spectrum. A straightforward computation of g_x and g_y shows that $g_x - g_y$ should be about 0.021 and the corresponding components should be quite well resolved. Since it is not the case, the following alternative seems more likely.

(ii) One of the components of the 12 000-cm^{-1} band could be a third intervalence transition, the other component and the 18 500-cm^{-1} band being the two d–d transitions. Since the electronic interaction between corner-sharing octahedra is important (see below), the excited state involved in the intervalence transition cannot be considered as localized on one molybdenum atom. Actually, the two d_{xy} orbitals of the two neighboring corner-linked molybdenum(VI) atoms interact, giving two excited levels (bonding and antibonding) separated by approximately $2J$ (twice the transfer integral).[48] Thus two distinct intervalence transitions can be expected for the "extra-group" process. One of them would contribute to the 7000–8000 cm^{-1} absorption (together with the "intra-group" band) and the second one would probably explain the shoulder near 11 500 cm^{-1}, this energy being rather low for a d–d transition.

It can be noticed that in both hypothesis i and ii the corner-shared triangular group of three MoO_6 octahedra would be the actual chromophore responsible of all the observed bands. This is strongly supported by the analogy between the spectra of $[XMo_{12}O_{40}]^{n-}$ and β-$[SiMo_3W_9O_{40}]^{5-}$ (see Figure 10).

Comparison of Thermal and Optical Energies for Electron Transfer: Electronic Interaction in the Lindqvist and Keggin Structures. As reported in the introduction, a comparison between thermal and optical activation energies will enable us to give an estimation of the transfer integral J.

The J values calculated by eq 1[49] are reported in Table IV, together with an indication of the temperature at which electron delocalization begins to broaden the ESR lines. In addition, we have given the J values obtained by assuming that the shoulder near 11 500 cm^{-1} could be assigned to a third intervalence transition. In this case, the separation between the two intervalence energies corresponding to the corner-linked octahedra is about $2J$. It can be seen that the J values obtained by these two independent methods are in reasonable agreement. The most striking feature of Table IV is the much higher transfer integral for dodecanuclear species with respect to $[Mo_6O_{19}]^{3-}$. In the calculations, this results from the particularly low E_{th} values in dodecanuclear species, as it appears that E_{op} values are not very different from one compound to another. The reasons for this particular behavior will now be discussed.

Let us consider a $Mo^{VI}O_6$ octahedron within a polyanion. A one-electron reduction gives rise to a Mo^{5+} ion, since according to ESR results, the unpaired electron is trapped at very low temperature on one molybdenum site. This is a self-trapping process in which the extra electron polarizes its surrounding and lowers the potential energy of the MoO_6 octahedron by a quantity W_p, where W_p is the so-called polaron binding energy.[42] During the optical transition, this polarization remains frozen according to the Franck–Condon principle, so that $E_{op} = 2W_p$.[42] Thus, the optical activation energy mainly depends on the polarization of the MoO_6 octahedra upon reduction and could in principle be calculated from bond-length variation between Mo^V and Mo^{VI} and force constants. It is not expected to depend very much on the interaction between two neighboring octahedra. This is actually what happens, Table IV showing that E_{op} and thus W_p do not vary by more than 20% from one species to one another. This presumably arises from the close analogy between MoO_6 units in the Keggin and Lindqvist structures.

On the contrary, the thermal activation energies spread over a much larger range, from 0.035 eV in the Keggin polyanion $[PMo_{12}O_{40}]^{4-}$ up to 0.155 eV in the Lindqvist $[Mo_6O_{19}]^{3-}$ polyanion. Indeed, the thermal energy barrier strongly depends on the electronic interaction which in turn depends on the way neighboring MoO_6 octahedra are linked. Table IV shows that this interaction is greater in the Keggin structure than in the Lindqvist one. This seems to be due to the corner-sharing mode of junction which is specific of the Keggin structure.

This conclusion appears nicely supported by the behavior of β-$[SiMo_3W_9O_{40}]^{5-}$ where the three MoO_6 octahedra are linked by corner sharing. In other respects, the electronic interaction

(45) For instance, the ligand field strength would be 8100 cm^{-1} in $[SiNi^{II}W_{11}O_{40}H_2]^{6-}$ vs. 8500 cm^{-1} in $[SiNi^{II}Mo_{11}O_{40}H_2]^{6-}$ (from the spectra given by the following: Weakley, T. J. R.; Malik, S. A. *J. Inorg. Nucl. Chem.* **1967**, *29*, 2935. Malik, S. A. *J. Inorg. Nucl. Chem.* **1970**, *32*, 2425). This is also consistent with ESCA measurements: Kazansky, L. P.; Feist, M.; Torcenkova, E. A.; Spitsyn, V. I. *Z. Anorg. Allg. Chem.* **1980**, *476*, 201. However, it should be pointed out that the reverse behavior (i.e., a greater ligand field strength for polytungstate) has been observed in $(Ni^{II}M_6O_{24}H_6)^{4-}$ (M = Mo, W): Baker, L. C. W. "Advances in the Chemistry of the Coordination Compounds"; Kirschner, S., Ed.; Macmillan: New York, 1961; p 610.

(46) In a previous report,[28] this band was not observed for $[SiMo_{12}O_{40}]^{5-}$, probably as a result of a bad performance of the spectrometer in the near-IR range.

(47) An alternative possibility would be to reverse the assignment between "intra-group" and "extra-group" transitions, as suggested by Tézé and Hervé.[20] We do not follow this point of view, since it would not explain the $[Mo_6O_{19}]^{3-}$ spectrum.

(48) This is confirmed by a theoretical analysis of the Mo_3 moiety reduced with one electron: Launay, J. P.; Babonneau, F. *Chem. Phys.*, in press.

(49) Strictly speaking, this equation is valid for a two-center system only. However, for systems containing more than two sites, the same qualitative trend is expected; i.e., any increase in the electronic interaction parameter would lead to a decrease in the activation energy.

appears to correlate well with the ground-state delocalization parameter β, which is lowest in the compounds containing corner-shared octahedra. It should be also mentioned that increasing the electronic interaction increases dramatically the intensity of all bands in the visible–near-IR spectra (Table II). This is shown by the large variation of the maximum extinction coefficient, which ranges from 340 mol^{-1} L cm^{-1} in $[Mo_6O_{19}]^{3-}$, to ~1300 mol^{-1} L cm^{-1} in $[XMo_{12}O_{40}]$ species.

Such a rough analysis does not take into account the nature of the central ion in the tetrahedral cavity. This ion appears to modify noticeably the structure of the polyanion and could thus play a role in the delocalization process. A more careful analysis should take into account not only the interaction between two neighboring molybdenum sites but the whole polyanion.

Acknowledgment. The technical assistance of F. Gatebled and D. Simons is gratefully acknowledged.

Registry No. $[MoW_5O_{19}]^{3-}$, 81193-94-4; $[Mo_6O_{19}]^{3-}$, 71767-69-6; $[SiMoW_{11}O_{40}]^{5-}$, 81218-89-5; $[PMo_{12}O_{40}]^{4-}$, 53850-86-5; $[AsMo_{12}O_{40}]^{4-}$, 76130-01-3; $[SiMo_{12}O_{40}]^{5-}$, 57656-95-8; $[GeMo_{12}O_{40}]^{5-}$, 76130-24-0; $[SiMo_3W_9O_{40}]^{5-}$, 81407-99-0; $[PMoW_{11}O_{40}]^{4-}$, 12776-99-7; $(NBu_4)_2[Mo_6O_{19}]$, 12390-22-6; $(NBu_4)_4[SiMo_{12}O_{40}]$, 59138-97-5; $(NBu_4)_4[GeMo_{12}O_{40}]$, 81205-59-6; $(NBu_4)_3[PMo_{12}O_{40}]$, 51542-98-4; $(NBu_4)_3[AsMo_{12}O_{40}]$, 81158-05-6; $(NBu_4)_4[SiMoW_{11}O_{40}]$, 68081-64-1; $K_8[SiW_{11}O_{39}]$, 37300-95-1; $K_4[SiMoW_{11}O_{40}]$, 81205-60-9; $(NBu_4)_4[SiMo_3W_9O_{40}]$, 81158-06-7; $Na_9[HSiW_9O_{34}]$, 81205-57-4; $(NBu_4)_3[MoW_5O_{19}]$, 81193-95-5; $H(NBu_4)_4[SiMo_3W_9O_{40}]$, 81423-62-3; $H_4[SiMo_3W_9O_{40}]$, 81407-98-9; Na_2MoO_4, 7631-95-0; Na_2GeO_3, 12025-19-3; MoO_3, 1313-27-5; As_2O_5, 1303-28-2; Na_2WO_4, 13472-45-2; WO_3, 1314-35-8.

Methylase Models: Studies on General-Base vs. Nucleophilic Catalysis in the Intramolecular Alkylation of Phenols

Jay O. Knipe, Peter J. Vasquez, and James K. Coward*

Contribution from the Department of Pharmacology, Yale University School of Medicine, New Haven, Connecticut 06510, and the Department of Chemistry, Rensselaer Polytechnic Institute, Troy, New York 12181. *Received August 31, 1981*

Abstract: The ortho substituted phenols, **1** and **3**, have been synthesized as models for the O-methylation of catecholamines, as catalyzed by catechol *O*-methyltransferase. The decomposition of **1** and **3** was studied at 40 °C over a wide range of pH in both oxyanion and amine buffers. Buffer catalysis of the reaction is observed, and product analyses show that oxyanion buffers catalyze a cyclization reaction to yield chroman (**4**) or 4,4-dimethylchroman (**5**), from **1** or **3**, respectively, in addition to *p*-nitrothioanisole (**6**). In contrast, amine buffers effect the intermolecular demethylation of **1** and **3**, to yield the corresponding *p*-nitrophenyl thioethers, **7** and **8**. The buffer-independent reaction involves cyclization to **4** or **5**, with formation of **6**. Brønsted β values of 1.1 and 0.89 for oxyanion-catalyzed reactions of **1** and **3**, respectively, are in contrast to the β value of 0.27 previously obtained in similar studies with a less acidic cyclopentanol substrate (*J. Am. Chem. Soc.* **1979**, *101*, 4339). However, other aspects of the oxyanion vs. amine buffer effects are in agreement with our earlier results and lead to the general conclusion that nucleophilic alkylation of alcohols and phenols is subject to general-base catalysis by oxyanion buffer species.

In a previous paper from this laboratory,[1] we demonstrated that several oxyanion buffers could act as general-base catalysts for the intramolecular alkylation of a cyclopentanol. Thus, related reactions of the type shown in eq 1 might be susceptible to similar

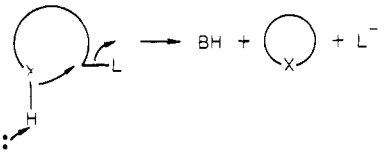

(1)

catalysis. However, the literature contains only one other reference to buffer catalysis of nucleophilic attack at sp^3 carbon; i.e., the borate-catalyzed cyclization of 4-chlorobutanol.[2] In another study,[3] no buffer catalysis was observed in the formation of chromans via intramolecular cyclization of (*o*-hydroxyphenyl)-propyl acetate, mesylate, etc. Thus, the generality of catalysis of nucleophilic reactions at sp^3 carbon remains to be explored.

Our own interest in the possibility of general-base-catalyzed nucleophilic displacement at sp^3 carbon arose from consideration of the substrate requirements and kinetic data for the enzyme-catalyzed methylation of catecholamines.[4] It was suggested that the enzyme, catechol *O*-methyltransferase (COMT, EC 2.1.1.6), might effect the transfer of a methyl group from the electrophilic donor, *S*-adenosylmethionine (SAM), to the nucleophilic acceptor, (nor)epinephrine, via general-base-catalyzed proton abstraction from one (or both) of the catechol hydroxyl groups. This is shown schematically in eq 2.

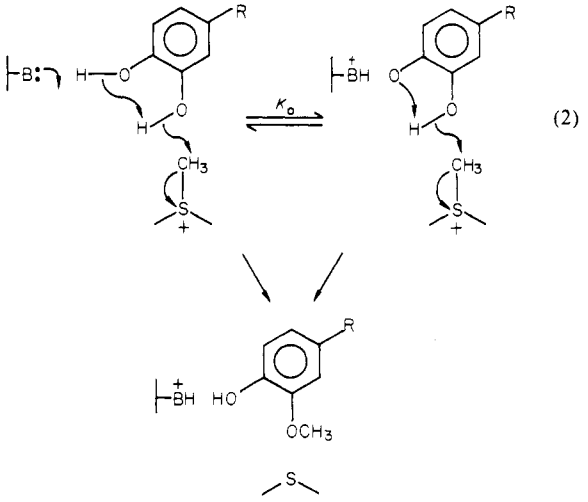

(2)

* To whom correspondence should be addressed at Rensselaer Polytechnic Institute.

(1) Knipe, J. O.; Coward, J. K. *J. Am. Chem. Soc.* **1979**, *101*, 4339–4348.
(2) Swain, C. G.; Kuhn, D. A.; Schowen, R. L. *J. Am. Chem. Soc.* **1965**, *87*, 1553–1561.
(3) Borchardt, R. T.; Cohen, L. A. *J. Am. Chem. Soc.* **1972**, *94*, 9166–9174.
(4) Coward, J. K.; Slisz, E. P.; Wu, F. Y.-H. *Biochemistry* **1973**, *12*, 2291–2297.

0002-7863/82/1504-3202$01.25/0